Polyelectrolyte Brushes with Added Salt

N. Arun Kumar and Christian Seidel*

Max-Planck-Institut für Kolloid- und Grenzflächenforschung, Am Mühlenberg, D-14476 Potsdam-Golm, Germany

Received July 19, 2005; Revised Manuscript Received August 26, 2005

ABSTRACT: Using molecular dynamics simulations, we study completely charged polyelectrolyte brushes with added salt at moderate electrostatic coupling strength. The full Coulomb interaction of monomers, counterions, and salt ions is treated explicitly. In the (nonlinear) osmotic brush regime, the brush thickness h is found to decrease with the salt concentration c_s, obeying a weak power law, $h \sim c_s^{-1/3}$. This result is in agreement with the scaling prediction by Pincus. The transverse ion distribution obtained in the simulations can be understood by means of a modified Donnan approach which takes into account the self-volume of polyelectrolyte chains.

I. Introduction

Polyelectrolytes constitute a very important class of polymers which has recently received considerable interest especially because of their importance in biology, materials science, and soft matter research.[1] Polyelectrolyte brushes consist of charged polymers densely end-grafted to surfaces of various geometries.[2] Here we restrict ourselves to the case of quenched polyelectrolytes end-tethered to a planar solid. However, weak polyelectrolyte brushes with an annealed charge distribution exhibit specific features.[3] Polyelectrolyte brushes form the subject of increasing interest by theory,[4−18] simulation,[19−24] and experiment.[25−39] From the application point of view polyelectrolyte brushes, e.g., are used for preventing colloids in polar media from flocculation[40] and in porous filters for pH-controlled gating.[41] Polyelectrolyte brushes are thought to be a model of the protecting envelope of cells (glycocalix).

According to Pincus,[13] the physics of polyelectrolyte brushes can be understood on the basis of a simple scaling theory. Let us assume that all counterions stay inside the brush layer, which is true if the Gouy−Chapman length $\lambda_{GC} = 1/(2\pi\lambda_B N f \rho_a)$ is small compared to the brush height h, with $\lambda_B = e^2/(4\pi\varepsilon_0\varepsilon k_B T)$ being the Bjerrum length, where ϵ_0 and ϵ are the vacuum permittivity and the dielectric constant of the solvent, respectively. Note that this assumption is reasonable for moderate Coulomb strength $u = \lambda_B/b \gtrsim 1$ and not too small grafting densities. In that situation the counterion concentration c_{ci} can be easily identified with the monomer concentration c_m by $c_{ci} = c_m f$, where f is the degree of charging. In the so-called osmotic brush regime the equilibrium brush height h is determined by the balance between the osmotic pressure of an ideal gas of counterions, $\pi_{ci} \simeq k_B T c_m f$, and the elasticity of a Gaussian chain, $\pi_{el} \simeq k_B T \rho_a h/(Nb^2)$, where b is the bond length, N the chain length, and ρ_a the grafting density. Assuming a steplike profile of the polymer concentration, one obtains

$$h \simeq Nbf^{1/2} \tag{1}$$

Using the strong-stretching entropic elasticity of a chain, the brush height in the osmotic regime becomes[12]

$$h \simeq Nb\,\frac{f}{1+f} \tag{2}$$

Note that in both cases the predicted brush height is independent of the grafting density ρ_a. However, including lateral inhomogeneities[12] or excluded-volume effects,[31] the brush height was theoretically shown to slightly increase with growing grafting density. This result is in agreement with simulations[24,31] as well as with recent experimental data.[31,39] For the nonlinear osmotic brush regime and in the high density, strong stretching limit theory predicts[31]

$$h \simeq Nb\,\frac{f+\sigma_{eff}{}^2\rho_a}{1+f} \tag{3}$$

where σ_{eff} effectively takes into account monomer and counterion diameters. A logarithmic dependence of the brush height on grafting density is produced by inhomogeneities of the counterion profile in the direction normal to the anchoring plane[10] which may be caused by diffusion of counterions outside the brush. However, for a large class of systems that are of interest in simulation[12] and experiment,[31] the percentage of counterions which diffuse outside is very small and can be neglected.

Varying salt concentration is an important parameter to tune structure and properties of polyelectrolytes. Both in experiment[32−39] and in theoretical work,[13−18] polyelectrolyte brushes with added salt form an interesting subject, where main attention is focused on the behavior of brush height and segment density profiles at varying salt concentrations. Several models have been proposed to understand the effect of additional salt on the brush height (for a brief review see, e.g., ref 35). The addition of monovalent salt of concentration c_s gives rise to a Debye screening length $\lambda_D = \kappa_s^{-1} = (8\pi\lambda_B c_s)^{-1/2}$. With an increase in the salt concentration, the Debye screening is expected to reduce the counterion osmotic pressure as $\pi_{ci} \simeq k_B T c_m f \kappa_0^2/\kappa^2$, where $\kappa_0^{-1} = (4\pi\lambda_B f c_m)^{-1/2}$ is the screening length associated with the counterions alone and $\kappa^2 = \kappa_0^2 + \kappa_s^2$. In the limit of $\kappa_s \gg \kappa_0$ the osmotic pressure becomes $\pi_{ci} \simeq k_B T c_m{}^2 f^2/c_s \simeq k_B T \upsilon_{eff} c_m{}^2$, which is basically the expression of a second virial

* Corresponding author. E-mail: seidel@mpikg.mpg.de.

10.1021/ma0515735 CCC: $30.25
Published on Web 10/04/2005

osmotic pressure. The effective excluded-volume parameter v_{eff}, however, now reads $v_{\text{eff}} \simeq f^2/c_s$, and the balance condition yields[13]

$$h \simeq Nb\left(\frac{\rho_a f^2}{bc_s}\right)^{1/3} \tag{4}$$

i.e., the brush height h decrease with c_s but only as a relatively weak power law. Later on the prediction has been confirmed and generalized by using refined theoretical approaches.[14−17] However, there is also a different prediction expecting a $h \sim c_s^{-2/3}$ scaling.[18]

Detailed simulations of polyelectrolyte brushes with added salt have not been reported so far. Because of the special methods required for treating the long-range Coulomb interaction, an increase of the total number of charges is rather expensive in computer time. However, molecular dynamics simulations of polyelectrolyte chains in solution with added salt have been recently performed.[42,43] To our knowledge there is one paper which reports a few simulation results on polyelectrolyte brushes with added salt, however, for a rather small system.[44]

In previous simulation studies, we investigated the structure of polyelectrolyte brushes in salt-free solution at varying grafting density and charge fraction, at both relatively strong and moderate electrostatic coupling.[23,24] Varying the Bjerrum length λ_B, a nonmonotonic behavior of the brush height is obtained. Furthermore, two novel brush regimes first obtained by simulation and having features not predicted by previous theories were reported: A collapsed regime where the brush thickness grows linearly with ρ_a is observed at rather strong electrostatic coupling.[23] Within an extended scaling theory which includes electrostatic correlations, it is understood that the collapsed brush regime can occur in the strong coupling limit $\lambda_B^3/v_2 > 1$ with v_2 being the second virial coefficient.[11] Reducing λ_B, the collapsed brush regime disappears[24,31] as predicted by the extended scaling model. However, contrary to the scaling law of the osmotic regime, the brush height exhibits still a weak dependence on ρ_a. As mentioned above, this behavior obtained also in experiments can be reproduced by allowing a laterally inhomogeneous distribution of counterions and/or taking into account the self-volume of polymers. The corresponding brush regime is called nonlinear osmotic.

In Figure 1 we plot the average height of chain ends $\langle z_e \rangle$ against the Bjerrum length λ_B, both in the case with and without added salt, for a polyelectrolyte brush with completely charged chains of length $N = 30$. In the nonlinear osmotic regime close to maximum stretching at $\lambda_B/b \approx 1$, we observe indeed a reduced brush height after adding salt. In the collapsed regime at large Bjerrum length, added salt reduces the attractive interaction that causes chain collapse. Thus, the brush becomes slightly swollen with additional salt.

The aim of this paper is to study the effect of added salt on completely charged polyelectrolyte brushes in the nonlinear osmotic brush regime. In particular, we examine the behavior of the brush thickness and segment density profiles on adding electrolyte. The Bjerrum length is set $\lambda_B = \sigma \approx b$, where σ is the Lennard-Jones length. The parameters of the underlying system are not changed compared to previous simulations[23,24] but extended to include monovalent completely ionized salt.

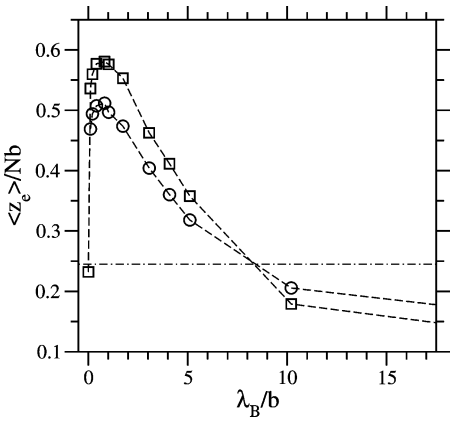

Figure 1. Average height of chain ends $\langle z_e \rangle$ for zero salt (squares) and with salt concentration $c_s\sigma^3 = 0.009$ (circles), both rescaled with the contour length Nb ($N = 30$), vs Bjerrum length λ_B at grafting density $\rho_a\sigma^2 = 0.02$. The dot−dashed line indicates $\langle z_e \rangle$ of an identical system of uncharged chains.

The paper is organized as follows. In the next section we introduce briefly the polyelectrolyte model and the simulation technique. The simulation results obtained for polyelectrolyte brushes with added salt are discussed in section III. Conclusions are given in section IV.

II. Simulation Model and Method

In this paper, we extend previous simulation work to include added salt. A detailed description of the model as well as of the simulation method can be found elsewhere.[23,24] Here we give only a brief survey of the basic elements. The brush is represented by M freely jointed bead−spring chains of length $N + 1$ which are anchored by one end to an uncharged planar surface at $z = 0$. Within the simulation box of size $L \times L \times L_z$ the grafting density is given by $\rho_a = M/L^2$. The uncharged anchor segments are fixed and form a square lattice with lattice spacing $d = \rho_a^{-1/2}$. For completely charged chains, due to electroneutrality there are $M \times N$ monovalent counterions. Additional salt ions of monovalent 1:1 type are modeled exactly in the same way as counterions.

The chains are assumed to be in a good solvent modeled by a purely repulsive short-range interaction that is described by a shifted Lennard-Jones potential U_{LJ}. Along the chains, beads are connected by a FENE bond potential U_{bond}. With our choice of parameters we obtain an average bond length $b \approx \sigma$, where σ is the Lennard-Jones parameter. All particles except the anchor segments are exposed to a short-ranged repulsive interaction U_{wall} with the grafting surface at $z = 0$. To reach a finite salt concentration, an identical wall is placed at the top boundary of the simulation box $z = L_z$.

Counterions and salt ions are treated as individual, nonbonded particles, and all charged entities interact with the bare Coulomb interaction

$$u_{\text{Coul}}(r) = k_B T q_i q_j \frac{\lambda_B}{r} \tag{5}$$

with q_i and q_j being the corresponding charges in units of elementary charge e.

It is well-known that the handling of long-range forces in simulations requires special methods.[50] To treat them

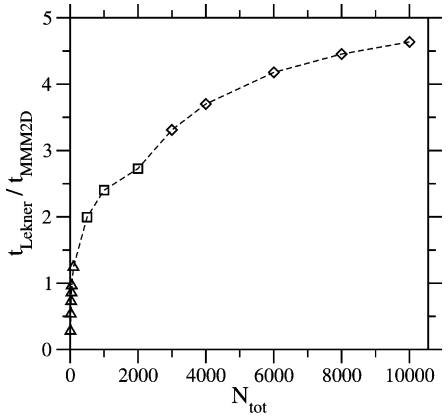

Figure 2. Performance gain between the MMM2D approach and Lekner's method measured by the relation between corresponding CPU times as a function of particle number N_{tot}. Different symbols correspond to a different number of layers the simulation box is subdivided in the MMM method: 8 (triangles), 16 (squares), and 32 (diamonds).

in the particular $2D + 1$ slab geometry (the simulation box is periodic only in x and y directions while perpendicular to the grafting surface the system is restricted to one layer), in previous simulations[11,23,24] we used a direct summation technique proposed by Lekner[45] and modified by Sperb.[46] This approach is, however, a so-called $\mathcal{O}(N_{tot}^2)$ method where the CPU time scales with the square of the number of particles N_{tot}. Unfortunately, such a behavior results in drastic restrictions on the maximum system size being accessible by simulation. In the new simulation code the Lekner method is replaced by the so-called MMM technique introduced by Strebel and Sperb[47] and modified for laterally periodic systems (MMM2D) by Arnold and Holm.[48] Although, due to symmetry breaking, the MMM scaling $\mathcal{O}(N_{tot} \log(N_{tot}))$ is not maintained in the $2D + 1$ case, the remaining $\mathcal{O}(N_{tot}^{5/3} \log(N_{tot})^2)$ behavior enables to increase significantly the total number of charged particles. Figure 2 shows the performance gain defined by the ratio of the corresponding CPU times as a function of particle number. Note that the dip at $N_{tot} \approx 2000$ is related to a change in the number of layers the simulation box is subdivided in the MMM method. Already for about 100 particles the MMM2D turns out to be faster than Lekner's method. The considerable performance gain allows to increase the maximum number of charges from about 2000 up to more than 7000. Finally, we are indeed able to add a sufficiently large number of salt ions to reach reasonable concentrations.

To study the system in equilibrium at constant temperature, we use stochastic molecular dynamics.[49,50] The equation of motion for particle i at position $\mathbf{r}_i(t)$ is the Langevin equation

$$m\frac{\mathrm{d}^2\mathbf{r}_i}{\mathrm{d}t^2} = -\nabla_i U - m\Gamma\frac{\mathrm{d}\mathbf{r}_i}{\mathrm{d}t} + \boldsymbol{W}_i(t) \tag{6}$$

where all particles carry the same mass m and Γ is a friction constant which couples the particles to a heat bath. U is the potential energy

$$U = U_{LJ} + U_{bond} + U_{wall} + U_{Coul} \tag{7}$$

The system is held at thermal equilibrium by a Gaussian random force $\boldsymbol{W}_i(t)$

$$\langle \boldsymbol{W}_i(t)\rangle = 0$$
$$\langle \boldsymbol{W}_i(t)\cdot\boldsymbol{W}_j(t')\rangle = 6mk_BT\Gamma\delta_{ij}\delta(t-t') \tag{8}$$

where the coupling to Γ is a consequence of the fluctuation−dissipation relation.

We used $m = 1$, $k_BT = 1.2\epsilon$, and $\Gamma = 0.5\tau_{LJ}^{-1}$ with $\tau_{LJ} = (m\sigma^2/\epsilon)^{1/2}$ being the Lennard-Jones time unit and ϵ is the Lennard-Jones energy. Equation 6 was integrated by means of the velocity-Verlet algorithm[50] with a time step $\delta t = 0.008\tau_{LJ}$. For a Newtonian trajectory with a quite similar time step, the total energy fluctuations have shown to be less than 10^{-4}.[23]

The sequential version of the molecular dynamics code with MMM2D implementation for evaluating long-ranged Coulomb interaction ran on local compute servers with Alpha EV67/667 and Intel XEON/3.06 processors. For using the IBM Regatta supercomputer the molecular dynamics code was parallelized by means of a self-scheduling (master-slave) algorithm.[51]

Two types of finite size effects may interfere with the simulation results discussed below. First, the chain length N should be long enough to capture typical polymeric behavior. Second, because of possible self-interaction of the chains, a small lateral system size due to the restricted number of chains M may also influence the large-scale properties such as brush thickness. In this study we have considered systems with $M = 36$ polyelectrolyte chains, each consisting of an uncharged fixed anchor and $N = 30$ negatively charged free chain monomers. With this particular choice of system size both types of finite size effects can be kept small.[23]

In previous simulations without additional salt ions there were no limitations of L_z, except arguments of numerical accuracy. Therefore, it could be chosen large enough that collisions of counterions with the top boundary of the simulation box were in fact rare events. For small Bjerrum lengths, however, the Gouy−Chapman length becomes large and L_z has to be taken of the order of some multiples of polymer contour length. Obviously, with added salt the situation is drastically changed because in any case a second wall potential at $z = L_z$ is necessary to maintain the desired finite salt concentration. On the other hand, box heights should be chosen as small as possible because additional salt ions will occupy preferentially the free space above the brush, and one would have to add a rather larger number before succeeding with a remarkable concentration within the brush. However, reducing L_z, a third kind of finite size effect might become important. To check this problem, we studied carefully the influence of a variation in box height on the structure of the brush. In Figure 3 the monomer density profiles are compared for three different heights L_z while all the other simulation parameters were kept constant. The plots are shown for two different salt concentrations. At the very tails, the profiles obtained with $L_z = 1.5N\sigma$ clearly deviate from those with $L_z = 3N\sigma$, indicating a finite size effect at box height $L_z = 1.5N\sigma$. The effect is enlarged with increasing salt concentration. On the other hand, a fairly good agreement is found between the profiles obtained for $L_z = 3N\sigma$ and $L_z = 2N\sigma$. Therefore, if not otherwise stated, we use a box height $L_z = 2N\sigma$ in the simulations reported here. Note that the suitability of the particular choice is also supported

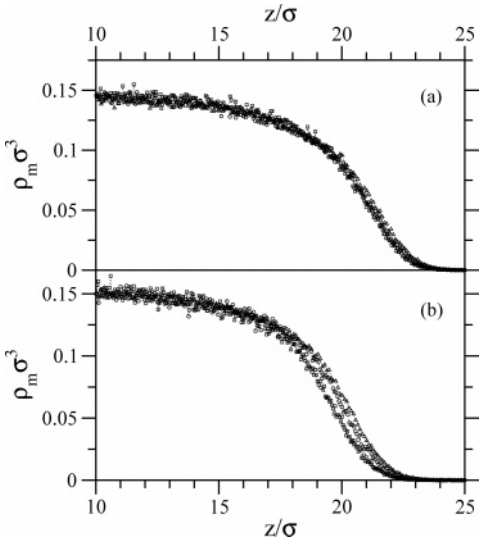

Figure 3. Monomer density $\rho_m(z)$ as a function of the distance from grafting surface at $\rho_a = 0.094\sigma^{-2}$ for three different box heights: $L_z = 1.5N\sigma$ (squares), $L_z = 2N\sigma$ (circles), $L_z = 3N\sigma$ (triangles). Shown is the outer part of the brush being eventually affected by the finite box height. (a) $c_s\sigma^3 = 0.016$, (b) $c_s\sigma^3 = 0.042$.

Table 1. Simulation Results on Completely Charged Polyelectrolyte Brushes with Varying Salt Concentration c_s ($\lambda_B = \sigma$): Average Brush Height $\langle z_m \rangle$, Average End-Point Height $\langle z_e \rangle$, Position of Inflection Point z_i, Ion Concentration Inside the Brush c''_{si}, and Buffer Concentration c'_{si} at Two Different Grafting Density ρ_a

$\rho_a\sigma^2$	$c_s\sigma^3$	$\langle z_m \rangle/\sigma$	$\langle z_e \rangle/\sigma$	z_i/σ	$c''_{si}\sigma^3$	$c'_{si}\sigma^3$
0.042[a]	0	9.55 ± 0.01	17.85 ± 0.03	20.5	0.059	0
0.042[a]	0.007	9.18 ± 0.01	16.98 ± 0.04	19.3	0.064	0.018
0.042[a]	0.014	8.88 ± 0.01	16.31 ± 0.04	18.4	0.072	0.034
0.042[a]	0.019	8.65 ± 0.01	15.72 ± 0.05	17.8	0.077	0.045
0.042[a]	0.028	8.30 ± 0.01	14.94 ± 0.03	16.7	0.088	0.066
0.042[a]	0.033	8.20 ± 0.01	14.83 ± 0.04	16.2	0.094	0.076
0.042[b]	0.007	9.15 ± 0.01	16.92 ± 0.04	19.2	0.065	0.021
0.042[b]	0.014	8.78 ± 0.01	15.97 ± 0.04	18.5	0.073	0.039
0.042[b]	0.021	8.46 ± 0.01	15.27 ± 0.04	17.8	0.081	0.055
0.042[b]	0.028	8.27 ± 0.01	14.78 ± 0.03	17.0	0.091	0.072
0.042[b]	0.035	7.98 ± 0.01	14.20 ± 0.04	16.2	0.101	0.087
0.042[b]	0.042	7.76 ± 0.01	13.65 ± 0.04	15.8	0.111	0.103
0.042[b]	0.049	7.63 ± 0.01	13.47 ± 0.05	15.7	0.122	0.118
0.094[a]	0	10.40 ± 0.01	19.72 ± 0.02	22.5	0.122	0
0.094[a]	0.016	10.16 ± 0.01	19.21 ± 0.03	21.5	0.129	0.042
0.094[a]	0.031	9.88 ± 0.01	18.57 ± 0.03	20.5	0.138	0.081
0.094[a]	0.042	9.73 ± 0.01	18.25 ± 0.03	20.0	0.147	0.106
0.094[a]	0.063	9.30 ± 0.01	17.28 ± 0.03	19.0	0.164	0.155
0.094[a]	0.073	9.13 ± 0.01	16.95 ± 0.03	18.5	0.174	0.179
0.094[b]	0.016	10.05 ± 0.01	18.96 ± 0.03	21.4	0.131	0.049
0.094[b]	0.031	9.78 ± 0.01	18.33 ± 0.03	20.3	0.142	0.093
0.094[b]	0.047	9.44 ± 0.01	17.56 ± 0.03	19.7	0.155	0.135
0.094[b]	0.063	9.12 ± 0.01	16.90 ± 0.03	18.7	0.170	0.173
0.094[b]	0.078	8.91 ± 0.01	16.41 ± 0.03	18.3	0.189	0.211
0.094[b]	0.091	8.73 ± 0.01	16.03 ± 0.03	18.0	0.206	0.239
0.094[b]	0.110	8.47 ± 0.01	15.38 ± 0.03	17.5	0.231	0.281

[a] Height of simulation box: $L_z = 3N\sigma$. [b] Height of simulation box: $L_z = 2N\sigma$.

by the scaling behavior discussed below where data obtained with both L_z equal to $2N\sigma$ and $3N\sigma$ are included (see Figure 7). The numerical results given in Table 1 show that, for different box heights, but at identical system parameters the average brush height differs by 2% at maximum; in a large range the difference is less than 1%.

Fully stretched chains with a line of counterions were used as initial configuration. The salt ions were distributed homogeneously in the simulation box. The relaxation was monitored by studying the decay of the end-point height of the chains. Details of the equilibration procedure can be found elsewhere.[23] As an additional check of equilibration, we considered two other initial configurations: one with all the salt ions confined above the fully stretched chains and another with all the salt ions completely inside the polymer layer. Both converged to the same equilibrium values as for the homogeneously distributed system. Typically, the relaxation of the brushes takes some hundreds of τ_{LJ}. After reaching equilibrium, we calculated trajectories between $2000\tau_{LJ}$ and $3000\tau_{LJ}$, depending on the anchoring density. With this trajectory lengths one can ensure that the relative error of the average height of chain ends is less than 1%. Errors were estimated by computing block averages[50] and by monitoring cumulative averages.[52]

Our model can be viewed as a coarse-grained representation of a flexible polyelectrolyte such as, e.g., poly(styrenesulfonate) (PSS). The length scale of the model is set by the Bjerrum length λ_B, which is about 0.7 nm for water at room temperature. Therefore, with the setting $\lambda_B = \sigma$, the average bond length b becomes ~0.7 nm, and the dimensionless Manning ratio is $\lambda_B/b = 1$, the same as the Manning condensation limit for a fully stretched chain. Using for PSS a monomer size of about 0.25 nm, one results with a fraction of charged monomer $f \approx 1/3$. In comparison, Manning theory predicts a charge faction $f = 0.25$ nm/0.7 nm = 0.35 for a fully stretched PSS chain in water.

III. Simulation Results and Discussion

A. Structure of the Brush. In this paper we present simulation results obtained at two different grafting densities $\rho_a = 0.042\sigma^{-2}$ and $0.094\sigma^{-2}$. Figure 4 shows a snapshot from the equilibrium trajectory for brushes at $\rho_a = 0.094\sigma^{-2}$ with salt concentration $c_s = 0.110\sigma^{-3}$. In this representation, the connectivity of the chains has been preserved, such that the chains may extend beyond the simulation box. Counterions are assigned to the closest chain monomer. In contrast to the saltless case, now the particle distribution looks rather homogeneous over the total height of the simulation box. Because in the present model polyelectrolyte counterions and salt counterions are considered to be identical, they are subject to an unrestricted exchange. As one can see from the snapshot, salt co-ions are diffusing into the brush layer. Although it cannot be seen directly in snapshots, due to local electroneutrality, these co-ions are escorted by a corresponding number of counterions. The different aspects of the ion distribution inside and outside the brush layer will be discussed below in detail.

The effect of added salt on the brush structure is shown in Figure 5. The monomer density $\rho_m(z)$ is plotted as a function of the distance from the grafting surface for the anchoring densities $\rho_a = 0.042\sigma^{-2}$ and $0.094\sigma^{-2}$. $\rho_m(z)$ is normalized such that $\int_0^\infty dz\rho_m(z) = N\rho_a$. From Figure 5, we learn (i) that chain stretching is slightly reduced with growing salt concentration and (ii) that the monomer density inside the brush is little increased with reduced stretching. These features are in agreement with the brush behavior in the (nonlinear) osmotic regime.

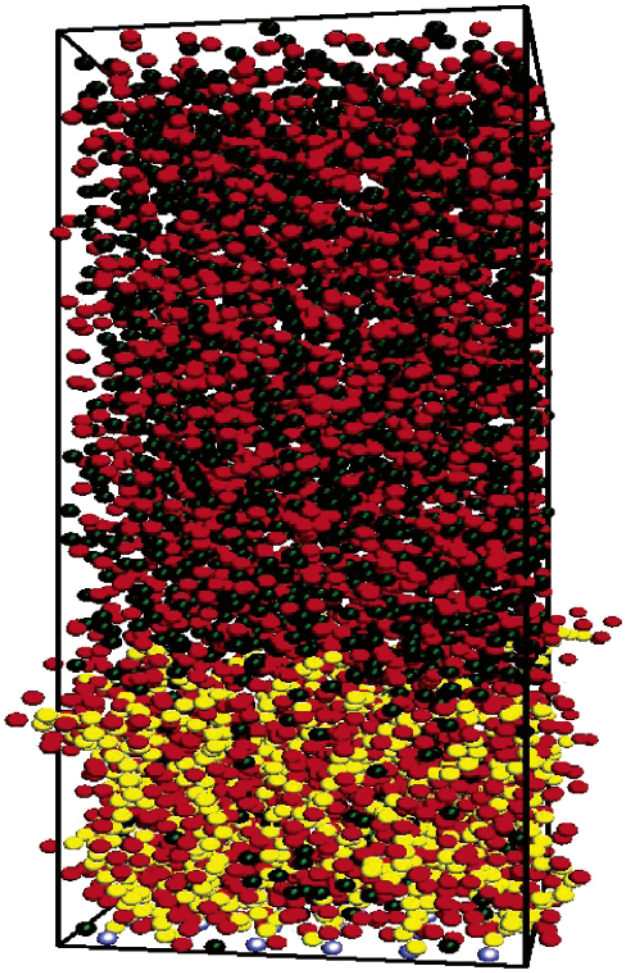

Figure 4. Polyelectrolyte brush with $M = 36$ chains of length $N = 30$, completely charged at grafting density $\rho_a\sigma^2 = 0.094$ with a salt concentration $c_s = 0.110\sigma^{-3}$ ($\lambda_B = \sigma$). Counterions in the brush are assigned to the closest chain monomer; polyelectrolyte chains are yellow (light gray), counterions and salt ions being oppositely charged as monomers are red (dark gray), likely charged salt ions are dark green (black), and anchor monomers are blue (gray with a spot). The box height perpendicular to the grafting surface is $L_z = 2N\sigma$. The snapshot out of a equilibrium trajectory has been represented by using the visualization program VMD.[53]

The average thickness of the brush is measured by taking the first moment of the monomer density profile

$$\langle z_m \rangle = \frac{\int_0^\infty z\rho_m(z)\,dz}{\int_0^\infty \rho_m(z)\,dz} \tag{9}$$

The average monomer heights for the systems considered in the present study (varying grafting density and salt concentration) are given in Table 1. To obtain an universal scaling curve, we follow a suggestion by Balastre et al.:[37] In Figure 6 we plot $h(c_s)/h_0$ vs $bc_s/(\rho_a f^{1/2})$. However, to rescale the brush height with a salt-free value h_0 instead of the osmotic brush height given in eq 1, we use that of the nonlinear osmotic brush given in eq 3, where the effective polymer thickness is set $\sigma_{eff}^2 = 2\sigma^2$.[31] Thus, all the data points fall indeed onto a universal curve in a log−log plot, which tends to a slope of zero in the low salt regime, indicating the validity of the nonlinear osmotic brush relation. Note that a simple estimation of the degree of condensed counterions by

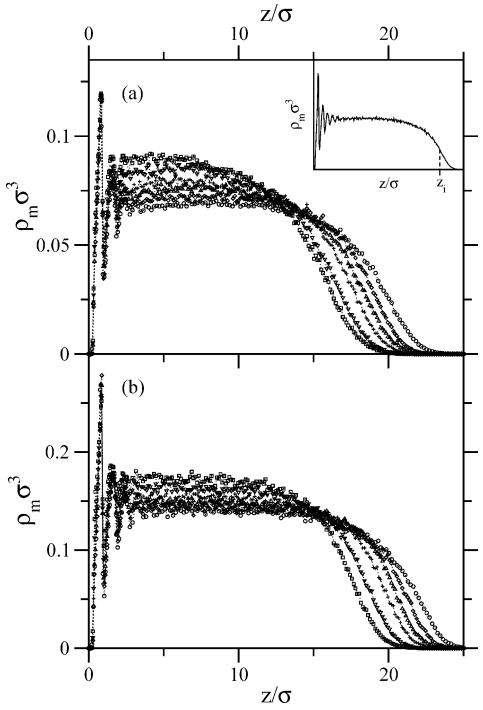

Figure 5. Monomer density profiles $\rho_m(z)$ of completely charged polyelectrolyte brushes ($N = 30$, $\lambda_B = \sigma$) as a function of the distance from the grafting surface: (a) at grafting density $\rho_a\sigma^2 = 0.042$ and varying salt concentration ($c_s\sigma^3 = 0$ (circles), 0.007 (diamonds), 0.014 (triangles up), 0.021 (plus), 0.035 (triangles down), 0.049 (squares)); (b) at grafting density $\rho_a\sigma^2 = 0.094$ ($c_s\sigma^3 = 0$ (circles), 0.016 (diamonds), 0.031 (triangles up), 0.047 (plus), 0.078 (triangles down), 0.110 (squares)). The inset shows schematically the estimation of inflection point z_i.

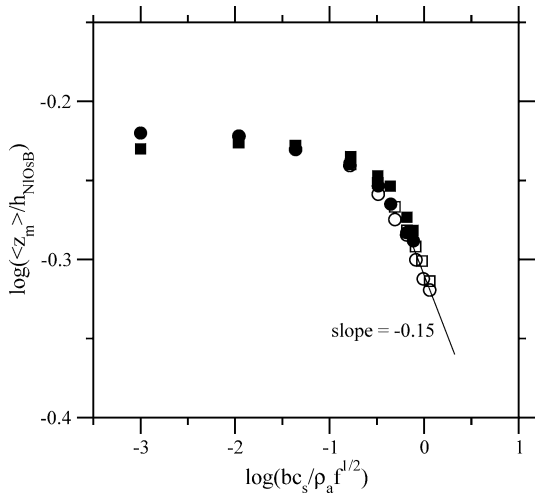

Figure 6. Salt concentration dependence of the brush height $\langle z_m \rangle$ ($\lambda_B = \sigma$, $f = 1$) as a master plot for two different grafting densities: $\rho_a = 0.042\sigma^{-2}$ (circles) and $0.094\sigma^{-2}$ (squares). Simulation results with $L_z = 2N\sigma$ (open symbols) and $3N\sigma$ (filled symbols). For the sake of representation, the asymptotic value at $c_s = 0$ is shown at $\log(bc_s/\rho_a) = -3$.

assuming them to be condensed if they are closer than λ_B yields $f_{eff} > 0.98$. That is why we assume $f = 1$ although the fraction of condensed counterions is slightly growing with increasing grafting density. On the other hand, obviously the limit of a salted brush, where the influence of counterions can be neglected, is not reached. A rough estimation yields that we are reaching the transition point $\pi_{ci} \approx \pi_s$ just at the highest salt concentrations, and the maximum negative slope found

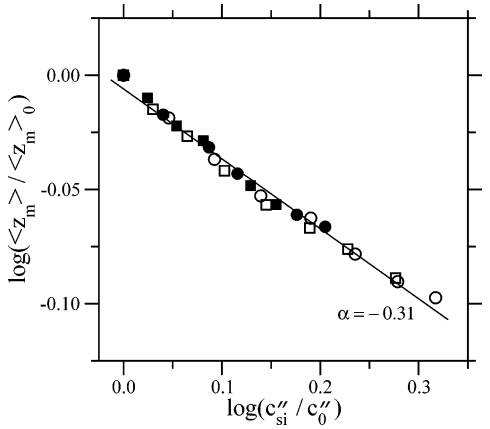

Figure 7. Average brush height $\langle z_m \rangle$ of completely charged polyelectrolyte brushes ($\lambda_B = \sigma$) vs the ion concentration inside the brush c''_{si} (both variables rescaled with the corresponding salt-free values $\langle z_m \rangle_0$ and c''_0, respectively). Symbols are the same as in Figure 6. The solid line shows a power-law fit.

in Figure 6 is about −0.15, i.e., roughly half of the value predicted by theory (see eq 4). However, a further increase of the total number of charges would enlarge the CPU time beyond a reasonable limit, and a reduced size of the simulation box would cause serious finite size effects. Thus, so far it seems hard to study the asymptotic salted brush regime $c_s \gg c_{ci}$ in simulations. Therefore, to account properly for the screening within the brush, the counterion concentration c_{ci} cannot be neglected.

To account for the concentration of mobile ions (chain counterions, salt counterions, and salt co-ions) which causes an effective screening inside the brush, we measure the brush height by the inflection point z_i, occurring in the monomer profile at the rim of the brush (see inset of Figure 5). Thus, the concentration of small ions inside the brush c''_{si} is obtained by counting the mobile ions within the layer $0 < z < z_i$. The corresponding values are also given in Table 1. On a log−log scale, in Figure 7, we plot the average brush height $\langle z_m \rangle$ vs the ion concentration inside the brush c''_{si}. Both $\langle z_m \rangle$ and c''_{si} are rescaled with the corresponding salt-free values $\langle z_m \rangle_0$ and c''_0, respectively. The brush height scales with c''_{si}, showing an exponent $\alpha \approx -0.31$. This result is in good agreement with the scaling law $h \sim c_s^{-1/3}$ predicted by Pincus for the salt dependence of the brush height in the osmotic regime.[13] Moreover, it is clear from Figure 7 that finite-size effects due to the setting $L_z = 2N\sigma$ do not affect, at least, the scaling behavior.

For a more detailed examination of the chain structure of grafted polyelectrolytes at all length scales, we calculate the spherically averaged single chain structure factor

$$S(q) = \left\langle \left\langle \frac{1}{N+1} \left| \sum_{j=0}^{N} \exp(i\mathbf{q}\mathbf{r}_j) \right|^2 \right\rangle_{|\mathbf{q}|} \right\rangle \qquad (10)$$

as well as the structure factor in transverse direction $S(q_z)$ and the in-plane averaged one $S(q_{xy})$. In analogy to free chains, in the asymptotic regime the structure factor is expected to obey the scaling relation $S(q) \sim q^{-1/\nu}$, where ν is the exponent of the N dependence of the chain radius $R \sim N^{\nu}$. Figure 8 gives the three different structure factors for the systems studied. Within the range of added salt for the two different

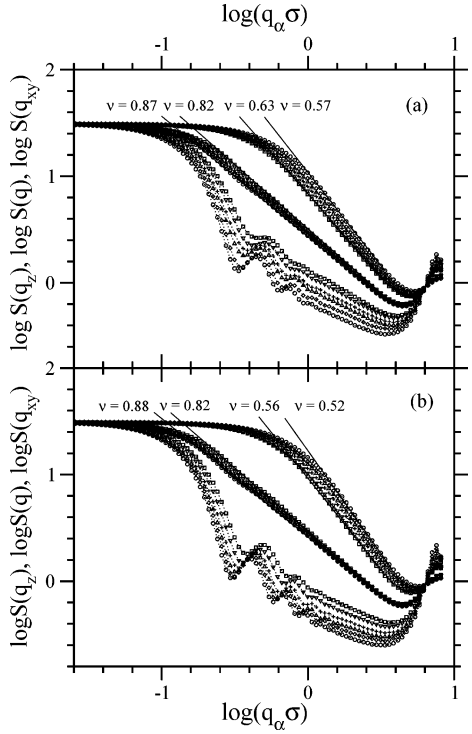

Figure 8. Spherically averaged structure factor $S(q)$ (middle set), in-plane averaged structure factor $S(q_{xy})$ (upper set), and structure factor perpendicular to the grafting plane $S(q_z)$ (lower set) of completely charged polyelectrolyte brushes ($\lambda_B = \sigma$): (a) grafting density $\rho_a = 0.042\sigma^{-2}$; (b) $\rho_a = 0.094\sigma^{-2}$. Symbols in (a) and (b) correspond to the same salt concentrations as in Figure 5, a and b, respectively.

anchoring densities studied, the spherically averaged structure factor $S(q)$ is almost not changed, reflecting strong stretching with Flory exponents in the range between 0.88 (no salt) and 0.82 (maximum salt). This result is consistent with the structure perpendicular to the grafting plane reflected by $S(q_z)$, which exhibits strong features of a rigid-rod-like behavior. However, the oscillations in $S(q_z)$ being related to ordering in z-direction get damped with increasing salt concentration, which is in agreement with the reduction in chain stretching obtained in Figure 5. The in-plane behavior of the grafted polyelectrolyte chains is determined by the properties of the underlying neutral chains. As expected for our model, which is supposed to mimic polyelectrolytes under good solvent conditions, at grafting density $\rho_a = 0.042\sigma^{-2}$ and without salt $S(q_{xy})$ exhibits an in-plane scaling $R_{xy} \sim N^{0.57}$, close to the good solvent value 0.6. At larger grafting density $\rho_a = 0.094\sigma^{-2}$, however, the salt-free $S(q_{xy})$ indicates $R_{xy} \sim N^{0.52}$, i.e., the scaling behavior of a Gaussian chain well-known for chains in melt. Independent of the anchoring densities, additional salt tends to shift the behavior toward that of a better solvent quality, i.e., the correlation length is slightly growing, and the blobs become a little more swollen.

B. Local Net Charge and Ion Distribution Close to Polyelectrolyte Chains. In previous studies we have shown that local electroneutrality is fulfilled in perpendicular direction over almost the total brush height, except (i) in a rather thin layer close to the interface and (ii) at the rim of the brush.[31] The local charge at small z is a consequence of the layering of monomers close to the grafting surface. The local net charge is compensated, however, over a length of the

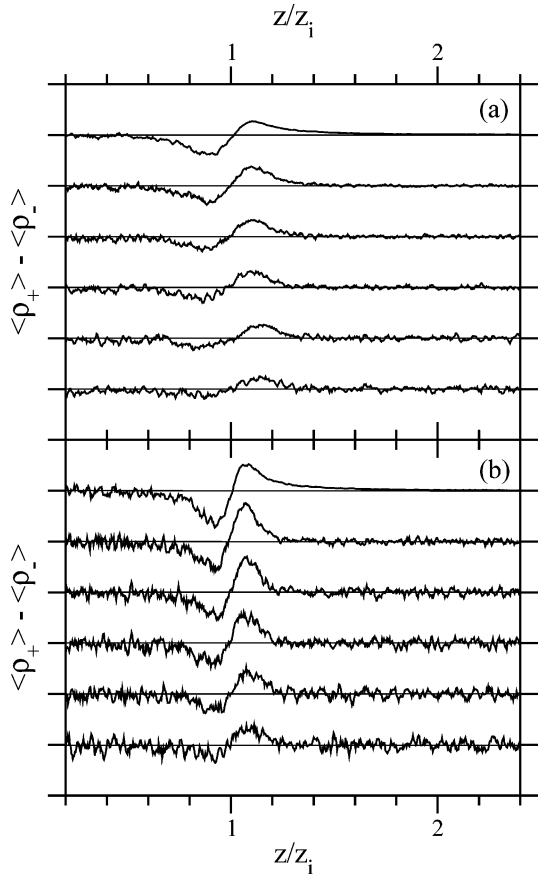

Figure 9. Local net charge $\langle\rho_+\rangle - \langle\rho_-\rangle$ as a function of the distance from grafting surface z (rescaled with the inflection point height z_i): (a) grafting density $\rho_a = 0.042\sigma^{-2}$; (b) $\rho_a = 0.094\sigma^{-2}$. Each curve corresponds to a certain salt concentration that is growing from top to down with the values given in Figure 5, a and b, respectively. In both subplots the topmost curve shows the saltless case, and each zero line is shifted by 0.02 in the y-direction.

order of bond length. In Figure 9 we plot the local net charge in layers parallel to the grafting plane as a function of their distance from that plane. For the sake of representation the region close to the anchoring points is omitted. Two features are evident: Except at the rim region $z \lesssim z_i$, one obtains only weak fluctuations around net charge zero. On the other hand, at the rim of the brush there appears a typical dipole with a depletion of counterions at $z \approx z_i$ and a corresponding enrichment beyond z_i. The strength of the dipole grows with grafting density while additional salt damps both the amplitude of local charges and its range in z-direction. Note that this dipole charge might have some influence on the interaction between two polyelectrolyte brushes.

In the osmotic regime, the overall structure of the brush is determined by the balance between the polymer elasticity and the counterion osmotic pressure. Debye screening caused by additional salt ions reduces the counterion osmotic pressure. To discuss the role of correlations and the degree of counterion condensation, we calculated the ion−polyelectrolyte distribution function $p(r)$ shown in Figure 10, where r is the separation between the center of a positive ion and the closest polyelectrolyte bond. The distribution $p(r)$ is normalized according to $2\pi f \int_0^\infty rp(r)\,dr = 1$. From Figure 10 we see that the strength of correlations is monotonically growing with both grafting density and salt concentration.

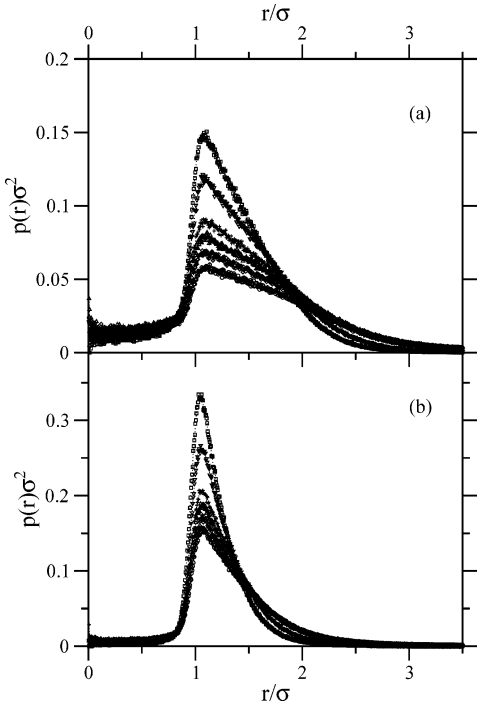

Figure 10. Ion−polyelectrolyte distribution function for completely charged chains ($\lambda_B = \sigma$): (a) grafting density $\rho_a = 0.042\sigma^{-2}$; (b) $\rho_a = 0.094\sigma^{-2}$. Symbols in (a) and (b) correspond to the same salt concentrations as in Figure 5, a and b, respectively. Note the different scale in the y-direction in (a) and (b).

Comparing this behavior with previous results at strong[23] and moderate[24] electrostatic coupling, we conclude that this is a fingerprint of simple packing effects. Although the chain stretching is slightly reduced with increasing salt concentration, giving rise to an increased effective line charge density of the polyelectrolytes, both the range of the distribution function and its amplitude indicate that counterion condensation does not give a significant contribution to the enhanced correlations.

C. Transverse Ion Distribution and Donnan Equilibrium. To get the relationship between the ion concentration inside the brush c''_{si} and the buffer concentration c'_{si} which is obtained by counting all the small ions above the inflection point z_i, in Figure 11 we plot the ratio c'_{si}/c''_{si} vs the salt concentration c'_s. From the point of view of the ion distribution perpendicular to the grafting plane a polyelectrolyte brush is very similar to the membrane equilibria problem where the membrane is impermeable to macroions but permeable to small ions. Hence, one can divide the simulation box into two compartments with the membrane "boundary" located at the rim of the brush that is defined in our model by z_i. Because of the presence of the macroions in one compartment, similarly charged ions are expelled from this compartment, giving rise to a somewhat nonhomogeneous distribution of the small ions as already pointed out by Donnan in 1911.[54,55] Applying the Donnan approach to the brush system, the ratio of the small ions in both compartments becomes

$$\frac{c'_{si}}{c''_{si}} = \left[1 + \left(\frac{fN\rho_a}{2z_i c'_s}\right)^2\right]^{-1/2} \tag{11}$$

with $fN = Q_p$ being the total charge of a polyelectrolyte chain and $\rho_a/z_i = c_p$ is the polymer concentration within the brush. Because we are considering systems char-

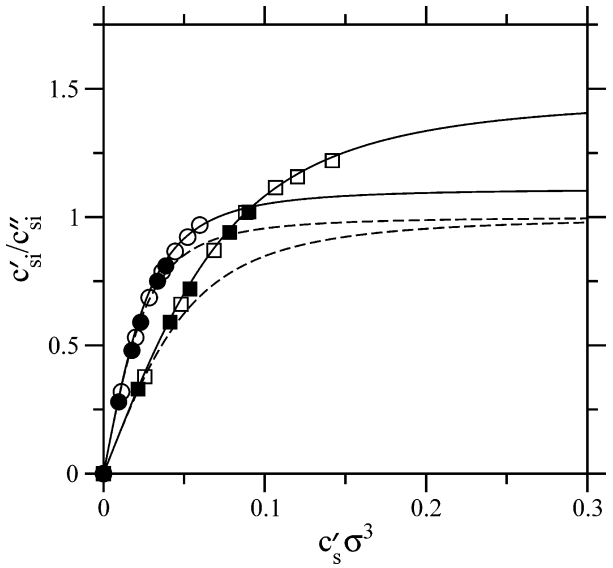

Figure 11. Relation between the ion concentration inside the brush c''_{si} and buffer concentration c'_{si} for different salt concentration c'_s. Simulation results (symbols as in Figure 6) and predictions of original (eq 11, dashed lines) and modified (eq 12, solid lines) Donnan approach.

acterized by very small Gouy−Chapman lengths $\lambda_{GC} \ll h$, all the counterions are basically trapped inside the brush. Therefore, the free ion concentration in the polymer-free volume can be set $c'_{si} = 2c'_s$. Although there occurs ion exchange between "original" counterions and salt counterions, due to electroneutrality such an approximation remains reasonable. Note, however, that because of the finite volumes considered in the simulations the salt concentration in the polymer free volume c'_s is larger than the bare salt concentration c_s (see Table 1). Equation 11 shows clearly the nonhomogeneous distribution of small ions. However, with increasing salt concentration the difference between the two compartments is compensated, and at $c_s \gg Q_p c_p$ one should obtain a uniform ion concentration $c'_{si} = c''_{si}$. In Figure 11, the predictions following from eq 11 are given by dashed lines. Obviously, the behavior disagrees with the simulation data that do not give a uniform ion concentration in the high salt limit. But we find a surplus of small ions on the polymer-free side that is growing with increasing grafting density, i.e., with enhanced polymer concentration.

Note that the Donnan effect has been evaluated for a system of pointlike constituents. While such an approximation is appropriate for dilute solutions, it fails for rather dense phases like polymer brushes. Recently, it has been shown that hard-core interactions between polymer monomers and counterions can be effectively taken into account within a free-volume approximation.[31] Here we use such an approximation to extend the Donnan equilibrium for dense solutions. The self-volume of the polymer is expressed in terms of an effective monomer hard-core diameter σ_{eff} and the polymer contour length Nb as $v = Nb\sigma_{eff}^2$, where σ_{eff} takes into account both the monomer and counterion/co-ion diameters. This yields the final expression

$$\frac{c'_{si}}{c''_{si}} = \frac{1}{1-\eta}\left[1 + \frac{1}{(1-\eta)^2}\left(\frac{fN\rho_a}{2z_i c'_s}\right)^2\right]^{-1/2} \qquad (12)$$

where $\eta = \rho_a Nb\sigma_{eff}^2/z_i$ gives the ratio of the polymer excluded volume v and the volume in the brush available for a polymer h/ρ_a with the brush height h being measured by the inflection point height z_i. Thus, η is the packing fraction of the polymer chain in the brush. (For a derivation of the above formula, see the Appendix.) Now both the asymptotic value of the ratio of the small ions at $c_s \gg Q_p c_p$ and the particular shape of the function on c_s depend on η, i.e., on anchoring density and chain stretching. Applying the same effective polymer thickness $\sigma_{eff}^2 = 2\sigma^2$ used in ref 31 to verify the weak dependence of brush height on grafting density, in Figure 11 the behavior following from eq 12 is given by solid lines. To obtain a continuous function, we have identified the inflection point z_i with the salt-free value z_i^0 although the brush height varies with salt concentration but, as discussed above, with a relatively weak power law $c_s^{-1/3}$. With these settings, we have packing fractions $\eta = 0.10$ and 0.32 for $\rho_a = 0.042\sigma^{-2}$ and $0.094\sigma^{-2}$, respectively, and the modified Donnan approach gives an almost perfect agreement with the simulation data.

IV. Conclusions

New molecular dynamics simulations of polyelectrolyte brushes with added salt are presented. In the nonlinear osmotic regime the brush is found to shrink with increasing electrolyte concentration. The scaling behavior of brush height is in almost perfect agreement with the prediction by Pincus for the salt dependence in the osmotic brush regime $\langle z_m \rangle \sim c_s^{-1/3}$. Note, however, that in the simulations we did not reach the asymptotic limit of the so-called salted brush where $c_s \gg c_{ci}$. Therefore, the contribution by the natural counterions cannot be neglected, but all mobile ions within the brush have to be taken into account. That is why we consider the brush stretching as a function of the concentration of mobile ions within the brush c''_{si} and not as a function of the salt concentration c_s only.

The relation between the total ion concentration in the brush c''_{si} and the buffer concentration c'_{si} at varying salt concentration c_s can be understood on the basis of an extended Donnan equilibrium approach. At high densities, as it is forced in polyelectrolyte brushes, the approximation of pointlike ions is not justified, but excluded-volume effects become relevant. Including the self-volume of the polyelectrolyte chains in a free volume approximation, very much in the spirit of the van der Waals equation, by defining an effective cross section σ_{eff}^2 that takes into account both the monomer and counterion size, we find a nice agreement with simulation results. The extended Donnan equilibrium relation represents a interesting theoretical prediction that should be checked by experimental data.

Acknowledgment. We gratefully acknowledge a grant for the IBM Regatta supercomputer at NIC Jülich, Germany. N.A.K. acknowledges Axel Arnold for helpful comments on his MMM2D code. We thank Roland Netz for useful discussions.

Appendix. Donnan Equilibrium for Polyelectrolyte Brushes

In the present analysis we consider the polyelectrolyte brush as a system that consists of two different solutions separated by a semipermeable membrane, permeable to small ions but not to macroions. As first pointed out in 1911 by F. G. Donnan,[54] the difference of the

electrostatic potential on both sides of the membrane causes a unequal distribution of the small ions.

Thermodynamic parameters on the polymer-free side will be designated by a single prime while doubly primed ones are related to the polymer-containing part. For simplicity, we are dealing with 1−1 electrolytes, and the macroion counterions are assumed to be identical to the salt counterions. Let us consider macroions of charge $Z = fN$ while M^+ and X^- are to refer to the small ions, both of originally counterions and of an added salt.

To study the thermodynamic behavior of electrolytes in solution, it is appropriate to express the composition of the solution not in terms of the ionic species but in terms of neutral components. A convenient definition uses the following three components: component 1—solvent (usually water); component 2—macroion + $Z/2$ ions X^- − $Z/2$ ions M^+; component 3—neutral salt, MX. Because we are interested in the equilibrium distribution of the small ions, here we focus the analysis on component 3. The condition for thermodynamic equilibrium is given by the equality of the corresponding chemical potentials

$$\mu_3' = \mu_3'' \tag{A1}$$

For simple 1−1 electrolytes, it is most convenient to transform eq A1 into a relation between activities a_i. On the side free from macroions, we have directly

$$\mu_3' = \mu_3^0 + RT \ln a_3' \tag{A2}$$

where μ_3^0 is the chemical potential at a reference state. Neglecting the effect of the osmotic pressure, which gives for reasonable parameters a change in a_3 of about 0.05%,[55] on the macroion containing side it holds a similar expression:

$$\mu_3'' = \mu_3^0 + RT \ln a_3'' \tag{A3}$$

Thus, eq A1 becomes simply

$$a_3' = a_3'' \tag{A4}$$

Since the activity of an electrolyte is the product of the constituent ion activities, $a_3 = a_+a_-$, eq A4 yields

$$a_+' a_-' = a_+'' a_-'' \tag{A5}$$

Replacing the activity by the product of ion concentration $c_\pm$ and ion activity coefficient $\gamma_\pm$, $a_\pm = c_\pm \gamma_\pm$, and assuming the same activity coefficients on both sides, eq A5 gives

$$\frac{n_+' n_-'}{(L_z - h)^2} = \frac{n_+'' n_-''}{h^2} \tag{A6}$$

where n_+' (n_-') and n_+'' (n_-'') are the number of positive (negative) ions in the polymer-free and polymer-containing side, respectively. The demarcation line between the two sides is given by the brush height h, which in our case is determined by the inflection point height z_i (see section IIIA). L_z is the total height of the simulation box. Additionally, we have the condition of electroneutrality on both sides, which gives

$$\frac{n_+'}{L_z - h} = \frac{n_-'}{L_z - h} \equiv \frac{c_s'}{\rho_a} \tag{A7}$$

and

$$n_+'' - n_-'' = fN \tag{A8}$$

respectively, where c_s is the salt concentration. The combination of eqs A6−A8 yields

$$n_+''^2 - fNn_+'' = c_s'^2\left(\frac{h}{\rho_a}\right)^2$$

$$n_-''^2 + fNn_-'' = c_s'^2\left(\frac{h}{\rho_a}\right)^2 \tag{A9}$$

Defining the corresponding concentrations of small ions by $c_{si}'' = (n_+'' + n_-'')\rho_a/h$ and $c_{si}' = (n_+' + n_-')\rho_a/(L_z - h)$, finally one obtains for the ratio of small ions on both sides

$$\frac{c_{si}'}{c_{si}''} = \left[1 + \left(\frac{fN\rho_a}{2hc_s'}\right)^2\right]^{-1/2} \tag{A10}$$

which represents the classical Donnan equilibrium expression for the particular brush system. Note the asymptotic behavior at large salt concentration where eq A10 gives $c_{si}' = c_{si}''$, i.e., a homogeneous distribution at the whole system. Obviously this prediction does not agree with our simulation results. Below we will see that the disagreement is related to the assumption of pointlike ions made in the derivation of eq A10.

In principle, the approximation used in the Donnan approach is a small density expansion that neglects second-virial interaction. To capture semiquantitatively the effect of that interaction, in the present analysis we use a free volume approximation very much in the spirit of the van der Waals equation for the liquid−gas transition. Recently the approach has been successfully used to understand experimental as well as simulation results, showing that in contrast to well-accepted scaling relations the height of polyelectrolyte brushes increases slowly as the grafting density goes up.[31] Within that approach we concentrate on the effective hard-core volume of a single polyelectrolyte chain v, which reduces the free volume that is available for the small ions. This free volume theory therefore takes the hard-core interaction between the polymer monomers and the small ions into account in a nonlinear fashion. Compared to that, the excluded-volume interaction between small ions is weak and will be neglected. Note that this approximation might fail at very high salt concentrations where the short-ranged ion−ion interaction is expected to give a noticeable contribution.

Because of the self-volume v the effective concentration of small ions on the polymer-containing side is growing as

$$c_i'' = \frac{n_i''}{V''} \Rightarrow \frac{n_i''}{V'' - v} \tag{A11}$$

with the bare volume in the brush available for a chain $V'' = h/\rho_a$. The self-volume of a polymer chain is roughly independent of the brush height and can be expressed in terms of the polymer contour length Nb and an effective monomer hard-core diameter σ_{eff} as $v = Nb\sigma_{eff}^2$, where σ_{eff} takes into account both the monomer and

counterion diameters. Thus, the effective concentration can be written

$$c_i'' = \frac{n_i''}{V''(1-\eta)} \tag{A12}$$

with $\eta = v/V'' = \rho_a \sigma_{eff}^2 Nb/h$ being the ratio of the polymer self-volume and the volume in the brush available for a chain and thus being the degree of close packing in the brush.

Using eq A12, the condition of equilibrium given in eq A6 becomes

$$\frac{n_+' n_-'}{(L_z - h)^2} = \frac{n_+'' n_-''}{h^2(1-\eta)^2} \tag{A13}$$

which yields together with the conditions of electroneutrality, eqs A7 and A8

$$n_+''^2 - fNn_+'' = c_s'^2\left(\frac{h(1-\eta)}{\rho_a}\right)^2$$

$$n_-''^2 + fNn_-'' = c_s'^2\left(\frac{h(1-\eta)}{\rho_a}\right)^2 \tag{A14}$$

Finally, the ratio of small ions on both sides reads

$$\frac{c_{si}'}{c_{si}''} = \frac{1}{1-\eta}\left[1 + \frac{1}{(1-\eta)^2}\left(\frac{fN\rho_a}{2hc_s'}\right)^2\right]^{-1/2} \tag{A15}$$

Hence, at a finite packing fraction η the distribution of the small ions at large c_s is never homogeneous, but it exhibits the asymptotic limit

$$\frac{c_{si}'}{c_{si}''} = \frac{1}{1-\eta} \tag{A16}$$

References and Notes

(1) Dautzenberg, H.; Jaeger, W.; Kötz, J.; Philipp, B,; Seidel, C.; Stscherbina, D. *Polyelectrolytes: Formation, Characterization and Application*; Hanser Publishers: Munich, 1994. Förster, S.; Schmidt, M. *Adv. Polym. Sci.* **1995**, *120*, 51−133. Barrat, J.-L.; Joanny, J.-F. *Adv. Chem. Phys.* **1996**, *94*, 1−66.

(2) Halperin, A.; Tirrell, M.; Lodge, T. P. *Adv. Polym. Sci.* **1991**, *100*, 31−71. Guenoun, P.; Argillier, J.-F.; Tirrell, M. *C. R. Acad. Sci. Paris, Ser. IV* **2000**, *1*, 1163−1169. Rühe, J.; et al. *Adv. Polym. Sci.* **2004**, *165*, 79−150. Naji, A.; Seidel, C.; Netz, R. R. *Adv. Polym. Sci.*, in press.

(3) Israëls, R.; Leermakers, F. A. M.; Fleer, G. J. *Macromolecules* **1994**, *27*, 3087−3093.

(4) Miklavic, S. J.; Marèelja, S. *J. Phys. Chem.* **1988**, *92*, 6718−6722.

(5) Misra, S.; Varanasi, S.; Varanasi, P. P. *Macromolecules* **1989**, *22*, 4173−4179.

(6) Borisov, O. V.; Birshtein, T. M.; Zhulina, E. B. *J. Phys. II* **1991**, *1*, 521−526.

(7) Ross, R. S.; Pincus, P. *Macromolecules* **1992**, *25*, 2177−2183.

(8) Wittmer, J.; Joanny, J. F. *Macromolecules* **1993**, *26*, 2691−2697.

(9) Amoskov, V. M.; Pryamitsyn, V. A. *J. Chem. Soc., Faraday Trans.* **1994**, *90*, 889−893.

(10) Zhulina, E. B.; Borisov, O. V. *J. Chem. Phys.* **1997**, *107*, 5952−5967.

(11) Csajka, F. S.; Netz, R. R.; Seidel, C.; Joanny, J.-F. *Eur. Phys. J. E* **2001**, *4*, 505−513.

(12) Naji, A.; Netz, R. R.; Seidel, C. *Eur. Phys. J. E* **2003**, *12*, 223−237.

(13) Pincus, P. *Macromolecules* **1991**, *24*, 2912−2919.

(14) Zhulina, E. B.; Borisov, O. V.; Birshtein, T. M. *J. Phys. II* **1992**, *2*, 63−74.

(15) Israëls, R.; Leermakers, F. A. M.; Fleer, G. J.; Zhulina, E. B. *Macromolecules* **1994**, *27*, 3249−3261.

(16) Borisov, O. V.; Zhulina, E. B.; Birshtein, T. M. *Macromolecules* **1994**, *27*, 4795−4803.

(17) Zhulina, E. B.; Wolterink, J. K.; Borisov, O. V. *Macromolecules* **2000**, *33*, 4945−4953.

(18) Argillier, J.-F.; Tirrell, M. *Theor. Chim. Acta* **1992**, *82*, 343−350.

(19) Granfeldt, M. K.; Miklavic, S. J.; Marèelja, S.; Woodward, C. E. *Macromolecules* **1990**, *23*, 4760−4768.

(20) Sjöström, L.; Åkesson, T.; Jönsson, B. J. *J. Chem. Phys.* **1993**, *99*, 4739−4747.

(21) Chen, H.; Zajac, R.; Chakrabarti, A. *J. Chem. Phys.* **1996**, *104*, 1579−1588.

(22) Csajka, F. S.; van der Linden, C. C.; Seidel, C. *Macromol. Symp.* **1999**, *146*, 243−249.

(23) Csajka, F. S.; Seidel, C. *Macromolecules* **2000**, *33*, 2728−2739.

(24) Seidel, C. *Macromolecules* **2003**, *36*, 2536−2543.

(25) Watanabe, H.; Patel, S. S.; Argillier, J. F.; Parsonnage, E. E.; Mays, J. W.; Dan-Brandon, N.; Tirrell, M. *Mater. Res. Soc. Symp. Proc.* **1992**, *249*, 255−265.

(26) Amiel, C.; Sikka, M.; Schneider, J. W.; Tsao, Y. H.; Tirrell, M.; Mays, J. W. *Macromolecules* **1995**, *28*, 3125−3134.

(27) Ahrens, H.; Förster, S.; Helm, C. A. *Macromolecules* **1997**, *30*, 8447−8452.

(28) Biesalski, M.; Rühe, J. *Macromolecules* **1999**, *32*, 2309−2316. Biesalski, M.; Rühe, J.; Johannsmann, D. *J. Chem. Phys.* **1999**, *111*, 7029−7037.

(29) Tran, Y.; Auroy, P.; Lee, L.-T.; Stamm, M. *Phys. Rev. E* **1999**, *60*, 6984−6990. Tran, Y.; Auroy, P. *Eur. Phys. J. E* **2001**, *5*, 65−79.

(30) Muller, F.; Fontaine, P.; Delsanti, M.; Belloni, L.; Yang, J.; Chen, Y. J.; Mays, J. W.; Lesieur, P.; Tirrell, M.; Guenoun, P. *Eur. Phys. J. E* **2001**, *6*, 109−115.

(31) Ahrens, H.; Förster, S.; Helm, C. A.; Kumar, N. A.; Naji, A.; Netz, R. R.; Seidel, C. *J. Phys. Chem. B* **2004**, *108*, 16870−16876.

(32) Guenoun, P.; Schlachli, A.; Sentenac, D.; Mays, J. W.; Benattar, J. J. *Phys. Rev. Lett.* **1995**, *74*, 3628−3631.

(33) Mir, Y.; Auroy, P.; Auvray, L. *Phys. Rev. Lett.* **1995**, *75*, 2863−2866.

(34) Ahrens, H.; Förster, S.; Helm, C. A. *Phys. Rev. Lett.* **1998**, *81*, 4172−4175.

(35) Hariharan, R.; Biver, C.; Mays, J.; Russel, W. B. *Macromolecules* **1998**, *31*, 7506−7513. Hariharan, R.; Biver, C.; Russel, W. B. *Macromolecules* **1998**, *31*, 7514−7518.

(36) Tran, Y.; Auroy, P.; Lee, L.-T. *Macromolecules* **1999**, *32*, 8952−8964.

(37) Balastre, M.; Li, F.; Schorr, P.; Yang, J.; Mays, J. W.; Tirrell, M. V. *Macromolecules* **2002**, *35*, 9480−9486.

(38) Kaewsaiha, P.; Matsumoto, K.; Matsuoka, H. *Langmuir* **2004**, *20*, 6754−6761.

(39) Romet-Lemonne, G.; Daillant, J.; Guenoun, P.; Yang, J.; Mays, J. W. *Phys. Rev. Lett.* **2004**, *93*, 148301.

(40) Napper, D. H. *Polymeric Stabilization of Colloidal Dispersions*; Academic Press: New York, 1983.

(41) Park, Y. S.; Ito, Y.; Imanishi, Y. *Chem. Mater.* **1997**, *9*, 2755−2758. Ito, Y.; Park, Y. S.; Imanishi, Y. *Langmuir* **2000**, *16*, 5376−5381.

(42) Stevens, M. J.; Kremer, K. *J. Chem. Phys.* **1995**, *103*, 1669−1690.

(43) Stevens, M. J.; Plimpton, S. J. *Eur. Phys. J. B* **1998**, *2*, 341−345.

(44) Terao, T. *Phys. Rev. E* **2002**, *66*, 046707−1.

(45) Lekner, J. *Physica A* **1991**, *176*, 485−498.

(46) Sperb, R. *Mol. Simul.* **1994**, *13*, 189−193; *Mol. Simul.* **1998**, *20*, 179−200.

(47) Strebel, R.; Sperb, R. *Mol. Simul.* **2001**, *27*, 61−74.

(48) Arnold, A.; Holm, C. *Comput. Phys. Commun.* **2002**, *148*, 327−348.

(49) Grest, G. S.; Kremer, K. *Phys. Rev. A* **1986**, *33*, 3628−3631.

(50) Allen, M. P.; Tildesley, D. J. *Computer Simulation of Liquids*; Oxford University Press: Oxford, 1987.

(51) Gropp, W.; Lusk, E.; Skjellum, A. *Using MPI*; The MIT Press: Cambridge, MA, 1994.

(52) Chandler, D. *Introduction to Modern Statistical Mechanics*; Oxford University Press: New York, 1987.

(53) Humphrey, W.; Dalke, A.; Schulten, K. *J. Mol. Graphics* **1996**, *14.1*, 33−38.

(54) Donnan, F. G. *Z. Elektrochem.* **1911**, *17*, 572.

(55) Tanford, C. *Physical Chemistry of Macromolecules*; John Wiley & Sons: New York, 1961.

MA0515735